

Magnetized tori in the background of a deformed compact object

Shokoufe Faraji* and Audrey Trova†

University of Bremen, Center of Applied Space Technology and Microgravity (ZARM), 28359 Germany

In this paper, we studied the relativistic accretion thick disc model raised by a deformed compact object up to the quadrupole moment. The goal of this work is to study the space-time and the effects of quadrupole moments via studying the properties of these equilibrium sequences of magnetized, non-self-gravitating discs in this space-time. We employed different angular momentum distributions and discussed the procedure of building this toroidal disc model based on a combination of approaches previously considered in the literature. We have shown the properties of this relativistic accretion disc model and its dependence on the initial parameters. Besides, this theoretical model can serve as the initial data for numerical simulations.

I. INTRODUCTION

Accretion disc is currently a topic of widespread interest in astrophysics that links different areas of research. In view of a general agreement, the observed properties of many astrophysical objects could be best explained in the framework of accretion disc. However, there is no unified theoretical accretion disc model which could explain all the basic properties of these sources and each of them just models some properties that are best fit to the observation. The investigation of the proper disc models, by analytical or numerical setup, rely on the ability of constructing suitable representations based on physical assumptions. Among this successful theoretical models is thick accretion disc with a toroidal shape and no magnetic field which was first introduced in 1974 and presented in these seminal works [1–8]. This model provides a general method to build equilibrium configurations of the perfect fluid matter orbiting around a stationary and axially symmetric black hole. After the confirmation of the significant role of magnetic field in astronomical phenomena in [9], [10] proposed a magnetic version of this model. This work involves an analytic solution for an axisymmetric, stationary torus with the constant specific angular momentum distribution and a toroidal magnetic field configuration. This simple analytical solution can serve as criterion for numerical MHD.

On the other hand, there are studies where considering different distributions of angular momentum in the discs instead of setting this to be fixed. [11] presented a method to build sequences of black hole tori in the dynamical equilibrium of the purely hydrodynamical case. [12] combine approaches considered in [10] and [11] to build new sequences of magnetic equilibrium tori around Kerr black holes. Also, [13] extended the original set of Komissarov' solutions in the presence of the particular case of power-law distributions of angular momentum, which is used in studying MRI instability through time dependent numerical simulations [14].

These mentioned works considered accretion onto the Kerr black hole. There are also studies on accretion disc models in different space-times. For example study the properties of accretion discs around naked singularities [15], or in wormhole space-times [16], in Schwarzschild-de Sitter

black holes [17], in Kerr-de Sitter backgrounds [18], in the Reissner-Nordström-(anti-)de Sitter space-times [19], in distorted Schwarzschild space-time [20], or by adding a cosmological constant [21].

In this work we generalized the extension of the models in some respects. First, combine the approaches described in [10], and [11]. Second, consider [10], and [13] to construct different magnetised disc models with non-constant angular momentum distributions, where in this procedure the location and morphology of the equipotential surfaces can be computed numerically. Third, in this work we construct these models in the space-time of a deformed compact object up to quadrupole moment, with the aim of study this solution via exploring the properties of magnetised tori in this background. We will see, for the particular case of vanishing quadrupole moment, the results are in good agreement with the mentioned papers.

This space-time is the simplest asymptotically flat solution of Einstein equation with quadrupole moment. In this respect, the first static and axially symmetric solution with arbitrary quadrupole moment is described by [22]. Then [23] introduced a static solution with arbitrary quadrupole in prolate spheroidal coordinates. Later [24] and [25] found an equivalent transformation that leads to a simple solution which can be treated analytically and is known as q-metric. In 1970, the relativistic multipole moments of vacuum static asymptotically flat space-time was introduced by [26], and later it was generalized to the stationary case by [27]. This area of study has been discussed extensively in the literature and generalized in many respects. For example, a general static axisymmetric solution in prolate spheroidal coordinate is discussed in [28], external field of static deformed mass in [29], derivation of source integrals for multipole moments in [30], motion around deformed centres in [31, 32], equatorial circular orbits in Weyl space-times in [33], stationary q-metric in [34], multipole moments in general relativity in [35], the QM solution which contains an infinite number of gravitational and electromagnetic multipole moments in [36], stationary solution with arbitrary multipole moment in [37], circular orbits in [38], among many others.

In this paper we restrict our attention to q-metric which describes the outer of a deformed compact object up to quadrupole. Also, we compare the results of non-constant angular momentum with the constant angular momentum distributions in both cases of spherical object and deformed object.

* shokoufe.faraji@zarm.uni-bremen.de

† audrey.trova@zarm.uni-bremen.de

The organization of the paper is as follows: the q-metric briefly presents in Section II. Section III presents an overview on the magnetised tori. While Section IV and V explain different distributions of angular momentum. The results and discussion are presented in Section VI. Finally, the conclusions are summarised in Section VII. In this paper, the geometrized units where $c = 1$ and $G = 1$, also the signature $(-+++)$ are used.

II. SPACE-TIME OF A DEFORMED COMPACT OBJECT

We have chosen to construct this magnetised tori model in the background of a deformed compact object with the quadrupole. We review this space-time briefly in this Section. In fact, it is convenient to study multipole moments via the Weyl metric which is written in the prolate spheroidal coordinates (t, x, y, ϕ) [23, 28],

$$ds^2 = -e^{2\psi} dt^2 + M^2 e^{-2\psi} \left[e^{2\gamma} \left(\frac{dx^2}{x^2-1} + \frac{dy^2}{1-y^2} \right) + (x^2-1)(1-y^2)d\phi^2 \right], \quad (1)$$

where $t \in (-\infty, +\infty)$, $x \in (1, +\infty)$, $y \in [-1, 1]$, and $\phi \in [0, 2\pi)$. Also, M is a parameter which may identify as the mass of the central object with the dimension of the length. This metric has two functions $\psi = \psi(x, y)$ and $\gamma = \gamma(x, y)$, where ψ plays the role of a gravitational potential.

The first solution which is obtained from the Weyl metric is the Schwarzschild solution, which only contains a mass monopole moment and it is simply achieved by substituting these two metric functions in the Weyl metric,

$$\begin{aligned} \psi_{\text{Sch}} &= \frac{1}{2} \ln \frac{x-1}{x+1}, \\ \gamma_{\text{Sch}} &= \frac{1}{2} \ln \frac{x^2-1}{x^2-y^2}. \end{aligned} \quad (2)$$

In addition, the relation of this coordinates to Schwarzschild coordinates is given by

$$\begin{aligned} x &= \frac{r}{M} - 1, \\ y &= \cos \theta. \end{aligned} \quad (3)$$

The next solution could be one related to the quadrupole moment which describes the exterior of a mass with quadrupole moment. This solution by using [24] and [25] approach, and a transformation of its parameter [39] is known as q-metric,

$$ds^2 = - \left(\frac{x-1}{x+1} \right)^{(1+q)} dt^2 + M^2 (x^2-1) \left(\frac{x+1}{x-1} \right)^{(1+q)} \left[\left(\frac{x^2-1}{x^2-y^2} \right)^{q(2+q)} \left(\frac{dx^2}{x^2-1} + \frac{dy^2}{1-y^2} \right) + (1-y^2)d\phi^2 \right]. \quad (4)$$

This metric can obtain by substitution of ψ and γ in the Weyl metric (1), with the following expressions [40]

$$\begin{aligned} \psi_q &= \frac{(1+q)}{2} \ln \frac{x-1}{x+1}, \\ \gamma_q &= \frac{(1+q)^2}{2} \ln \frac{x^2-1}{x^2-y^2}. \end{aligned} \quad (5)$$

This metric is an axially symmetric exact vacuum solution of the Einstein field equation with a central curvature singularity at $x = -1$ and a naked singularity at $x = 1$. However, considering relatively small quadrupole moments, a physically reasonable interior solution can cover the singularities in such a way that out of this region the metric is asymptotically flat [41]. Therefore, this solution may describe the exterior gravitational field of a deformed compact object up to the quadrupole. By Geroch definition [26], the lowest independent multipole moments, monopole, for this metric is calculated as follows

$$m_0 = M(1+q), \quad (6)$$

where m_0 is taken to be positive in order to avoid a negative mass distribution, which determines the valid domain for the quadrupole as $q \in (-1, \infty)$ [42]. Also, the second multipole moment is calculated as [26],

$$m_2 = -\frac{M^3}{3} q(1+q)(2+q), \quad (7)$$

where constitutes the deviations from the spherically symmetric shape of the central compact object. It turns out that the only independent parameters are M and q which determine the mass and quadrupole moment. In addition, all the odd multipole moments vanish due to the reflection symmetry with respect to the equatorial plane.

Indeed, we can calculate all necessary quantities to construct this disc model in this space-time, in particular the Keplerian angular momentum

$$\ell_K = M(x-1) \left(\frac{x+1}{x-1} \right)^{q+\frac{3}{2}} \sqrt{\frac{1+q}{x-(1+q)}}, \quad (8)$$

In what follows we explain magnetised tori and different angular momentum distributions, respectively. In addition, in order to be compatible with this space-time we present the structure of magnetised tori also in this coordinates system. However, one can easily transform them to the spherical coordinates by using (3).

III. MAGNETISED TORI

Thick disc model presents a general method of constructing perfect fluid equilibria of matter in an axially symmetric

and stationary space-time, which is the best for model discs with no accretion flow, also radiatively inefficient. However, accretion rates can be very high ($\dot{m} \gg 1$), but the efficiency drops accordingly to very low values ($\eta_{\text{acc}} \ll 1$). Indeed, this toroidal model is the relevant framework to describe properties of the astrophysical object, where the radial pressure gradients can not easily negligible and they contribution leads to a significant growth in the vertical size of the disc. Here we briefly explain the magnetised version of thick discs which is a generalization of this model developed by [10].

The evolution of an ideal magnetised fluid describes by the following conservation laws; baryon conservation, energy-momentum conservation and induction equation [43, 44], respectively they read as

$$\nabla_\nu (\rho u^\nu) = 0, \quad (9)$$

$$\nabla_\nu T^{\nu\mu} = 0, \quad (10)$$

$$\nabla_\nu {}^*F^{\nu\mu} = 0, \quad (11)$$

where $T^{\mu\nu}$ is the total energy-momentum tensor of the fluid and electromagnetic field together, when the variation in pressure and density are adiabatic [43],

$$T^{\nu\mu} = (w + |b|^2) u^\nu u^\mu + \left(p_{\text{gas}} + \frac{1}{2} |b|^2 \right) g^{\nu\mu} - b^\nu b^\mu, \quad (12)$$

here p_{gas} is the gas pressure, u^μ is the four-velocity of the fluid, where b^μ is the four-vector magnetic field that is related to the magnetic pressure in the fluid as $|b|^2 = 2p_m$. Also, ${}^*F^{\nu\mu}$ is the Hodge dual Faraday tensor

$${}^*F^{\nu\mu} = b^\nu u^\mu - b^\mu u^\nu. \quad (13)$$

We proceed here following [10], by assuming purely rotational fluid motion and purely toroidal magnetic field,

$$u^x = u^y = b^x = b^y = 0. \quad (14)$$

In fact, with these simplified assumptions, the only job is to solve the energy-momentum stress conservation. Following [45] by choosing to have $\Omega = \Omega(\ell)$ as the integrability condition, the relativistic Euler equation by considering the projection of conservation of energy-momentum tensor into the plane normal to four-velocity is written as

$$\frac{1}{w} \nabla_i p = -\nabla_i \ln u_t + \frac{\Omega \nabla_i \ell}{1 - \Omega \ell} - \frac{\nabla_i \tilde{p}_m}{\tilde{w}}, \quad (15)$$

where i is x or y , also we have

$$\tilde{p}_m = \mathcal{L} p_m, \quad \tilde{w} = \mathcal{L} w, \quad (16)$$

where $\mathcal{L} = g_{t\phi}^2 - g_{t\phi} g_{\phi\phi}$. According to the definition of the specific angular momentum ℓ and the angular velocity Ω , we have

$$\ell = -\frac{u_\phi}{u_t}, \quad \Omega = \frac{u^\phi}{u^t}, \quad (17)$$

and their relationship as

$$\ell = -\frac{\Omega g_{\phi\phi} + g_{t\phi}}{\Omega g_{t\phi} + g_{tt}}, \quad \Omega = -\frac{\ell g_{tt} + g_{t\phi}}{\ell g_{t\phi} + g_{\phi\phi}}. \quad (18)$$

Moreover, u_t is the corresponding redshift factor

$$(u_t)^{-2} = -\frac{\ell^2 g_{tt} + 2\ell g_{t\phi} + g_{\phi\phi}}{g_{t\phi}^2 - g_{tt} g_{\phi\phi}}. \quad (19)$$

Adopting [10], we assume the equations of state for fluid and for magnetic field as

$$p = K w^\kappa, \quad \tilde{p}_m = K_m \tilde{w}^\eta \quad (20)$$

where K , κ , K_m and η are constants. Thus, we obtain

$$\int_0^p \frac{dp}{w} + \int_0^{\tilde{p}_m} \frac{d\tilde{p}_m}{\tilde{w}} = -\ln |u_t| - \ln |(u_t)_{in}| + \int_{\ell_{in}}^\ell \frac{\Omega d\ell}{1 - \Omega \ell}, \quad (21)$$

where the subscript *in* refers to the inner edge of the disc. The constant of integration was chosen in such a way that on the surface of the disc and its inner edge, i.e, $u_t = (u_t)_{in}$, and $\ell = \ell_{in}$, we have vanishing pressures.

In fact, by considering these particular choices of polytropic equations of state, the von Zeipel theorem [46] is fulfilled, and the equation (21) can fully integrate

$$W - W_{in} + \frac{\kappa}{\kappa - 1} \frac{p}{w} + \frac{\eta}{\eta - 1} \frac{p_m}{w} = \int_{\ell_{in}}^\ell \frac{\Omega d\ell}{1 - \Omega \ell}, \quad (22)$$

where $W = \ln |u_t|$. This equation implies $\Omega = \Omega(\ell)$ and the surface of equal Ω , ℓ , p and ρ coincide [45]. So, if one specifies $\Omega = \Omega(\ell)$, one can construct this model by solving equation (18) for Ω or ℓ and then $W(x, y)$ and $p(x, y)$ easily are followed. Also, one needs to specify $\ell(x, y)$ to fix the geometry of the equipotential surfaces which is discussed in the following Section.

IV. CONSTANT ANGULAR MOMENTUM

Of course the simplest assumption is when considering the constant specific angular momentum $\ell = \ell_0$, and then the right hand side of the equation (22) vanishes,

$$W - W_{in} + \frac{\kappa}{\kappa - 1} \frac{p}{w} + \frac{\eta}{\eta - 1} \frac{p_m}{w} = 0. \quad (23)$$

So the disc centre is at the larger radius for which ℓ_0 intersects with the local Keplerian angular momentum, and when ℓ_0 is bigger than the radius of the marginally stable Keplerian orbit ℓ_{ms} [10]. Then in this case, the disc surface is fully determined by the choice of W_{in} and it is independent of magnetic field [47], and the value of ℓ_0 determines the total potential

$$W(x, y) = \frac{1}{2} \ln \left| \frac{\mathcal{L}}{\mathcal{A}} \right|, \quad (24)$$

where $\mathcal{A} = g_{\phi\phi} + 2\ell_0 g_{t\phi} + \ell_0^2 g_{tt}$. For the different value region of ℓ_0 , we have [45],

$$\begin{cases} W_{\text{in}} \leq W_{\text{cusp}} & \text{if } |\ell_{\text{ms}}| < |\ell_0| < |\ell_{\text{mb}}|, \\ W_{\text{in}} < 0 & \text{if } |\ell_0| \geq |\ell_{\text{mb}}|, \end{cases} \quad (25)$$

Then the gas pressure and magnetic pressure at the centre c , become

$$p_c = w_c (W_{\text{in}} - W_c) \left(\frac{\kappa}{\kappa - 1} + \frac{\eta}{\beta_{\text{mc}}(\eta - 1)} \right)^{-1}, \quad (26)$$

where the subscript c refers to the mentioned quantities at the centre. Also, the magnetisation parameter β_{mc} is the ratio of the gas pressure to magnetic pressure at the centre. In summary, the variables of model are W , w , p , p_m , u^t , u^ϕ , b^t and u^ϕ . So by using equations of state, one can find K and K_m , then the solution is easily obtains via (22) and (24) [10].

V. NON-CONSTANT ANGULAR MOMENTUM

In this Section we briefly explain two models for angular momentum distribution introduced in [13] and [11], which we consider in this paper.

A. Power-law angular momentum

As a first case of non-constant angular momentum distribution following [13], we have assumed the angular velocity is a power-law function of specific angular momentum $\Omega = \Omega(\ell)$, which is a reasonable assumption from a mathematical point of view. We have

$$\Omega(\ell) = c\ell^n. \quad (27)$$

In fact, this is always the case considering pure rotation and a barytropic equation of state. Thereafter, the equation (22) can be written as [13]

$$\begin{aligned} W - W_{\text{in}} + \frac{\kappa}{\kappa - 1} \frac{p}{w} + \frac{\eta}{\eta - 1} \frac{p_m}{w} \\ = \frac{1}{n + 1} \ln \left(\frac{c\ell_{\text{in}}^{n+1} - 1}{c\ell^{n+1} - 1} \right). \end{aligned} \quad (28)$$

In order to find ℓ one needs to calculate parameters c and n . These are simply obtained when one has places of centre of the torus x_c and the cusp x_{cusp} . This means that by calculating $\Omega(x_c)$ and $\Omega(x_{\text{cusp}})$ and using the relation (18), we have easily these parameters and then the angular momentum distribution is followed [13]. It is worth to mention that for a perfect fluid rotating on circular geodesics, the shapes and location of the equipressure surfaces $p(x, y) = \text{constant}$, follow directly from the assumed angular momentum distribution and not depend on the equation of state, and the assumed entropy distribution [3].

B. Trigonometric function angular momentum

The second model for non-constant angular momentum that we have considered, is presented in [11]. This is a reasonable assumption from a physical point of view. Following them we have assumed an angular momentum distribution for the hydrodynamical case given by

$$\ell(x, y) = \begin{cases} \ell_0 \left(\frac{\ell_K(x)}{\ell_0} \right)^\alpha (1 - y^2)^\delta, & x \geq x_{\text{ms}}, \\ \ell_0 (\zeta)^{-\alpha} (1 - y^2)^\delta, & x < x_{\text{ms}}, \end{cases} \quad (29)$$

where $\ell_0 = \zeta \ell_K(x_{\text{ms}})$, and ℓ_K is the Keplerian angular momentum in the equatorial plane. Also, for the MHD case

$$\ell(x, y) = \begin{cases} \ell_0 \left(\frac{\ell_K(x)}{\ell_0} \right)^\alpha (1 - y^2)^\delta, & x \geq x_{\text{ms}}, \\ \ell_{\text{ms}}(x)(1 - y^2)^\delta, & x < x_{\text{ms}}, \end{cases} \quad (30)$$

where $\ell_{\text{ms}}(x)$ is calculated on the equatorial plane via considering Ω_{ms} simply by using equation (18). In this model, the parameters α , δ , and ζ are determined by these bounds

$$0 \leq \alpha \leq 1, \quad -1 \leq \delta \leq 1, \quad -1 \leq \zeta \leq \frac{\ell_K(x_{\text{mb}})}{\ell_K(x_{\text{ms}})}. \quad (31)$$

In this case, the equipressure surface which starts from the cusp is the marginally bound for $\alpha = \delta = 0$, and $\zeta = \frac{\ell_K(x_{\text{mb}})}{\ell_K(x_{\text{ms}})}$.

This procedure is described as follows. By utilizing twice the equation (15) for $i = x$ and $i = y$, and divide the two equations we get this relation for a static space-time [11],

$$\frac{\partial_x p}{\partial_y p} = \frac{\partial_x g^{tt} + \ell^2 \partial_x g^{\phi\phi}}{\partial_y g^{tt} + \ell^2 \partial_y g^{\phi\phi}} := -F(x, y) \quad (32)$$

Therefore, the function F is known once we have angular momentum distribution ℓ . In addition, if we take $y = y(x)$ as the explicit equation for the equipressure surface, this equivalent to have

$$\frac{dy}{dx} = F(x, y). \quad (33)$$

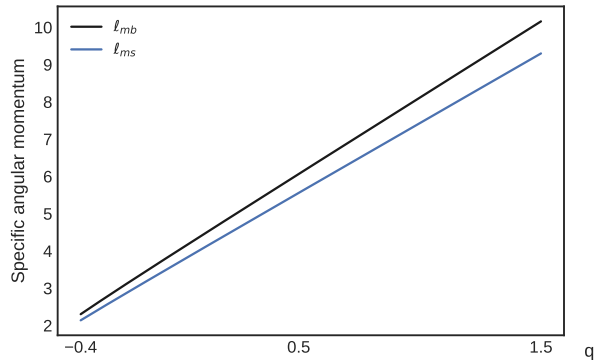


FIG. 1. Variation of ℓ_{mb} and ℓ_{ms} as a function of q which determines the area for existence of closed equipotential surfaces.

In fact, for a known angular momentum distribution, function F is given, and one may solve this equation to obtain y for different initial conditions, and therefore one can acquire all the possible locations for the equipressure surfaces by computing the integration of this function.

In what follows we present the results and discussion of configuration of the magnetised tori in the target space-time.

VI. RESULTS AND DISCUSSIONS

In this Section, we discuss various results showing the impact of the deformation of the compact object due to quadrupole moments, and the other parameters of the model on the location and morphology of the equipotential surfaces.

One of the determinant factors in this model is the condition on the existence of the closed equipotential surfaces, which is the case for having the angular momentum distribution in this range: $\ell_{ms} < \ell < \ell_{mb}$, as it was mentioned before. In this respect, Figure 1 gives us an insight on how the specific angular momentum at the marginally bound orbit ℓ_{mb} and at the marginally stable orbit ℓ_{ms} , behaves as a function of the deformation parameter q . Also, Figure 1 shows that by increasing q , the area where equipotential surfaces can exist, increases.

In this Section, the plots are presented in the (x, y) coordinates. Besides, we considered 5 different values of the deformed parameter, namely $q = 0$, which corresponds to the spherical compact object, the two negative values $q = -0.4$ and $q = -0.2$, and two positives values $q = 0.8$ and $q = 1.5$.

A. Discussion of the power-law angular momentum

In this subsection we present the results of considering [10] approach combined with angular momentum distribution introduced in [13]. The method is briefly described in Section V A. In fact, this model consists of choosing a fixed ℓ_0 specific angular momentum, which is going to fix the position of the cusp and the centre of the disc. As it has shown in Figure

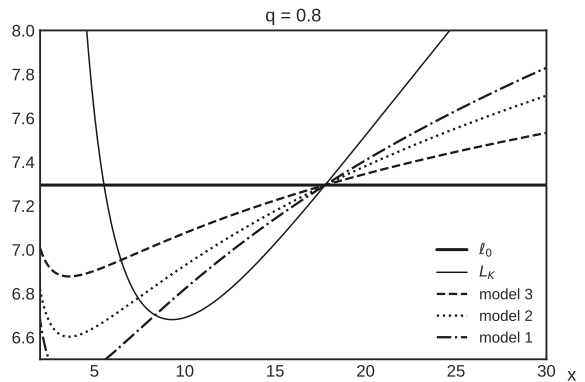


FIG. 2. The curves 1, 2 and 3 are profiles of the specific angular momentum in the equatorial plane with different slopes. The constant specific angular momentum is shown with the solid straight line which is chosen to be $\ell(x, y) = \ell_0 = \ell_{mb}(q)$. This profile corresponds to $q = 0.8$.

1, it is challenging to set a fixed value of ℓ which covers all the ranges of q value, therefore we chose to fix $\ell_0 = \ell_{mb}$ to have the same procedure for all models. The approach proceeds as follows. The centre x_c was fixed and we have created a new point called x'_{cusp} settled between x_{cusp} and x_{ms} . Using those two points, we can build a non-constant specific angular momentum distribution. An example of ℓ -profile in the equatorial plane is given for $q = 0.8$ in Figure 2.

We have built three different angular momentum profiles via choosing three different values of x'_{cusp} . The profiles are denoted by 1, 2 and 3 in Figure 2, where through the paper, we have referred to these profiles by model 1, 2 and 3 for all the tested q values. Besides, we have depicted the constant angular momentum distribution $\ell = 0 = \ell_{mb}$ for the sake of comparison.

In fact, the value of x'_{cusp} and x_c depend on q . As a result, the slope of the three models are going to depend on q as well. For all the plots in this section, the solid line is corresponding to the constant angular momentum case, the dashed line to the model 3, the dotted line to the model 2, and the model 1 is represented by the dot-dashed line.

We have started our inspection by considering the effects of different angular momentum distributions, and the effect of the magnetic field by means of parameter β_c . By its definition the lower β_c , corresponds to the stronger magnetic pressure. In this regard, our aim is to study the impact of the magnetic pressure on the characteristics of the disc, for various values of q , when this is strong in comparison to the gas pressure.

In Figure 3 we have represented the location and the amplitude of the rest-mass density as a function of the magnetisation parameter, for these five values of q mentioned before and for the four profiles of angular momentum, namely the constant angular momentum, and models 1, 2 and 3.

On one hand, for any fixed value of q , the location of the maximum of the rest-mass density by decreasing the value of β_c -increasing the magnetic pressure- is moving in the in-

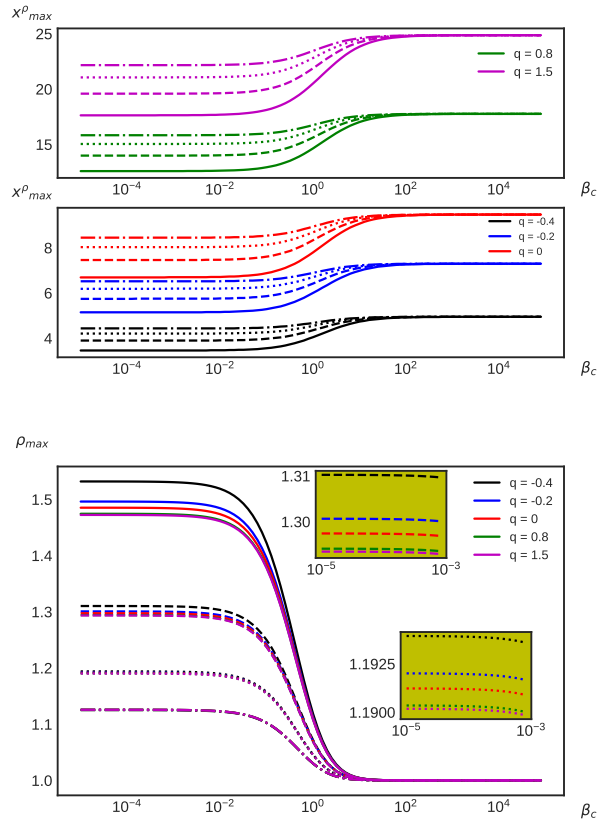


FIG. 3. Variation of the location and the maximum of the rest-mass density in the equatorial plane as a function of β_c for distribution profiles of specific angular momentum described in Figure 2.

wards direction. Moreover, the steeper is the density distribution profile, the further is the maximum of the rest-mass density. Thus, the steepness of angular momentum and the β_c parameter act contrariwise. Also, in Figure 3, if we concentrate on any chosen value of q , we can see that the four curves representing different models are coinciding when β_c is high, equivalently the magnetic pressure is low. Indeed, when β_c is low, the equipotential surfaces are not coinciding anymore with the equidensity surfaces. Also, decreasing β_c makes the maximum of the rest-mass density higher, and then its location closer to the central object for all models and quadrupole values. This effect is coherent with the results of the previous studies [10, 12].

On the other hand, the negative values of q cause the maximum of rest-mass density to happen closer to the central object and vice versa for positive values. In summary, the effects of steepness and positivity of quadrupole parameters are aligned and opposite to the negativity of quadrupole values and β_c .

To have a better insight on how the deformation parameter q , affects on the disc, in Figure 4 we have plotted the amplitude and the location of the rest-mass density for all models and a fixed chosen value of β_c . Figure at the top also confirms the results on Figure 3. In fact, as we have seen, the parameter

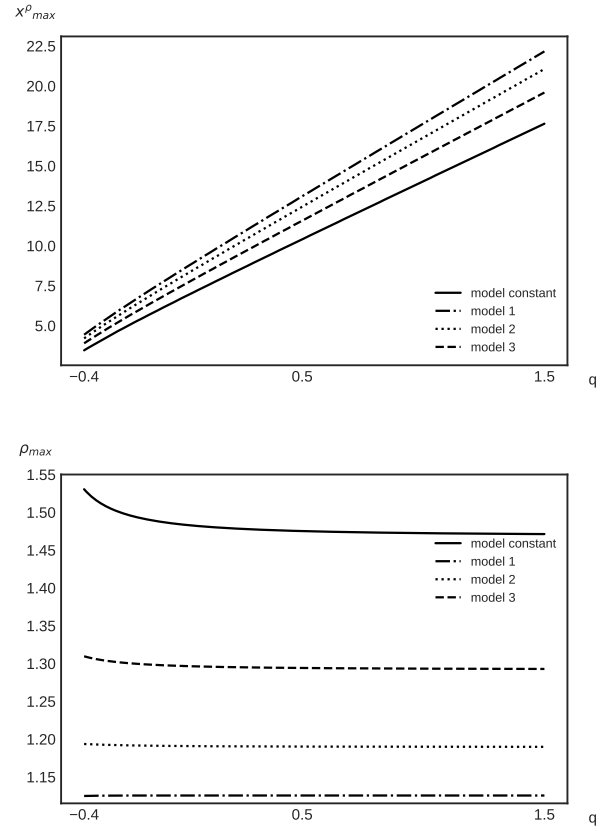


FIG. 4. Variation of the location and maximum of the rest-mass density in the equatorial plane as a function of q for distribution profiles of specific angular momentum described in Figure 2. The magnetisation parameter is set to be $\beta_c = 10^{-3}$.

q has a stronger impact on the position of maximum rest-mass density than the steepness of the angular momentum profile. However, it has a minor effect on the amplitude rather than two other mentioned parameters, which is depicted at the bottom.

In Figures 5 and 6, we have analysed the physical structure of the disc by building the panel of the rest-mass density distribution. Figure 5 shows how the disc structure is changing with the magnetisation parameter and with the steepness of the angular momentum profile for a fixed negative value of $q = -0.4$. columns represent different magnetisation parameters. The column at the left shows $\beta_c = 10^{-3}$, in the middle $\beta_c = 1$ and at the right depicts $\beta_c = 10^3$. This means the magnetic field is decreasing from the left to the right. Also, each row consistency with the different angular momentum distributions. The first row presents constant angular momentum $\ell = \ell_0$, the second row model 3, the third row model 2, and the last row the model 1.

The higher magnetic pressure, which is consistent with the low values of β_c , is pushing the matter in the inwards direction with respect to the central object. Thus, the matter will be more concentrated in the inner part of the disc. This pattern repeats for all the profiles of angular momentum distributions.

This is also coherent with the results found in the previous Figures. In general, the magnetisation parameter has a major effect on how the matter is distributed in the disc but has a minor effect on the geometrical structure of the disc.

On the other hand, considering different angular momentum profiles, we have different shapes and sizes of the disc through the panel. In fact, the steeper is the angular momentum profile, the less the disc is extended in the both directions. This result is coherent with the fact that the steeper the profile, the closer x_{cusp} and x_c to each other. Eventually, on the panel as we have expected from Figure 3 and 4, the matter distribution is more spread in the entire disc when the steepness is high and the magnetic field is less, namely β_c is high.

In addition, in Figure 6 we have considered the impact of the deformation parameter q together with the effect of different slopes of angular momentum profiles for a fixed value of β_c which corresponds to a stronger magnetic pressure in our models. In this Figure, the rows are depicted the variation of the slope as in the previous panel. However, each column represents a different value of q , starting with a negative value $q = -0.4$ at the left, $q = 0$ at the centre and a positive value $q = 1.5$ at the right. As it is seen, the deformation parameters have a minor effect on the overall shape of the disc. In fact, they are more relevant for the radial extension, namely an increase in q value corresponds to an increase in the radial extension of the disc. Moreover, we can mention, the concentration of the matter in the disc is not a function of q , and matter occupies the same percentage of the disc for any chosen value of q . This confirmed the fact that the amplitude of the rest-mass density is weakly influenced by the value of the deformed parameter as we have seen previously.

B. Discussion of the Trigonometric function angular momentum

In this subsection we describe the results of considering [10] approach incorporate with the angular momentum distribution presented in [11] and described in Section VB. We have shown different angular momentum profiles given by different combinations of the parameters.

In Figure 7, we have discussed the location of the positions for x_{cusp} and x_c as a function of different profiles and different quadrupole values q . In Figure 7, the dashed line x_c , is not changing with changing the profile; however, it is expected to vary with q . On the contrary, x_{cusp} is not fixed and changes with different profiles. Furthermore, both x_{cusp} and x_c are increasing functions of q . Thus, we expect that in the profiles for where the area between x_{cusp} and x_c shrinks, the size of the discs become smaller, namely for smaller quadrupole values.

In fact, we are interested in exploring the effects of the magnetisation parameter, q and different profiles of angular momentum, on the variation of the location and amplitude of the maximum rest-mass density. As it is shown in Figure 8, we have focused on three different profiles of the angular momentum, namely ($\alpha = \delta = 0$), i.e., constant case colored in black, ($\alpha = \delta = 0.5$) colored in red, and ($\alpha = \delta = 0.9$) colored in blue. It is worth mentioning that the α parameter is

the one more responsible for the location and amplitude of the rest-mass density and δ has an effect on the distribution of equidensity surfaces.

As the same as the previous model -the power-law angular momentum- for any fixed value of q , the location of the maximum comes closer to the central object by decreasing β_c , equivalently by increasing magnetic pressure; however, the strength of the effects in this model is different. Furthermore, in this model the location is also an increasing function of the parameter α . In fact, for small values of β_c the effect of changing the profile of angular momentum has the weaker effects in comparison to changing the value of quadrupole. Therefore, by considering Figures 7 and 8, we expect that by increasing the parameters β_c , α , δ , and q , the disc shrinks in the radial direction. About the amplitude, as for power-law profiles, it is a decreasing function of β_c , q and α . However, for small values of β_c this time changing in q has a minor effect, while the profile of the angular momentum has an intense impact. Indeed, the impact of the deformed parameter q is less and less manifest when we increase α . We can conclude that an increase in β_c , q or α , spreads the matter in a way that they are more concentrated in the middle of the disc that we see this more clearly in Figures 10 and 11.

In Figure 9, for a fixed chosen value of β_c we have studied the effect of q for the different angular momentum profiles. We have chosen $\beta_c = 10^{-3}$, where the magnetisation of the disc is high. We see that the location of the rest-mass density maximum is moving outwards with increasing q and α , which confirms the result from Figure 8. However, this shift is more significant for a higher value of α . The amplitude has an opposite behaviour, it decreases when both q and α increases, confirming also Figure 8. We should note that as for the power-law distribution the deformed parameter has a rather minor impact on the amplitude.

Further, we have built the solutions with this angular momentum ansatz and produced two panels of the rest-mass density in Figure 10 and Figure 11.

In Figure 10, the map is plotted with a fixed chosen value of $q = -0.4$, and for the different values of the magnetisation parameter and different angular momentum distributions.

As it has been shown also in the power-low case, the higher the magnetisation, the more accumulated the rest-mass density distribution in the inner part of the disc. Also, β_c does not change the shape of the disc. Then, as in Figure 8, we expected that the matter would be more spread in the entire disc when we increase β_c . This expectation is confirmed with the structure of the discs in this panel. Further, if we take a look at the panel from the top to the bottom, the structure of the discs are different. It is important to mention that the rows 1 and 4 have the same parameter $\alpha = 0$, which means they have the same location and amplitude of the rest-mass density maximum. The same discussion applies to rows 3 and 5 which they have shared the parameter $\alpha = 0.9$. In fact, an analysis shows that the α parameter is more responsible for the vertical direction of the disc in the way that as much as we increase α we have a less vertically extended disc. While, parameter δ effects on both the radial and the vertical extension of the disc. Also, it has an effect on the distribution of equidensity

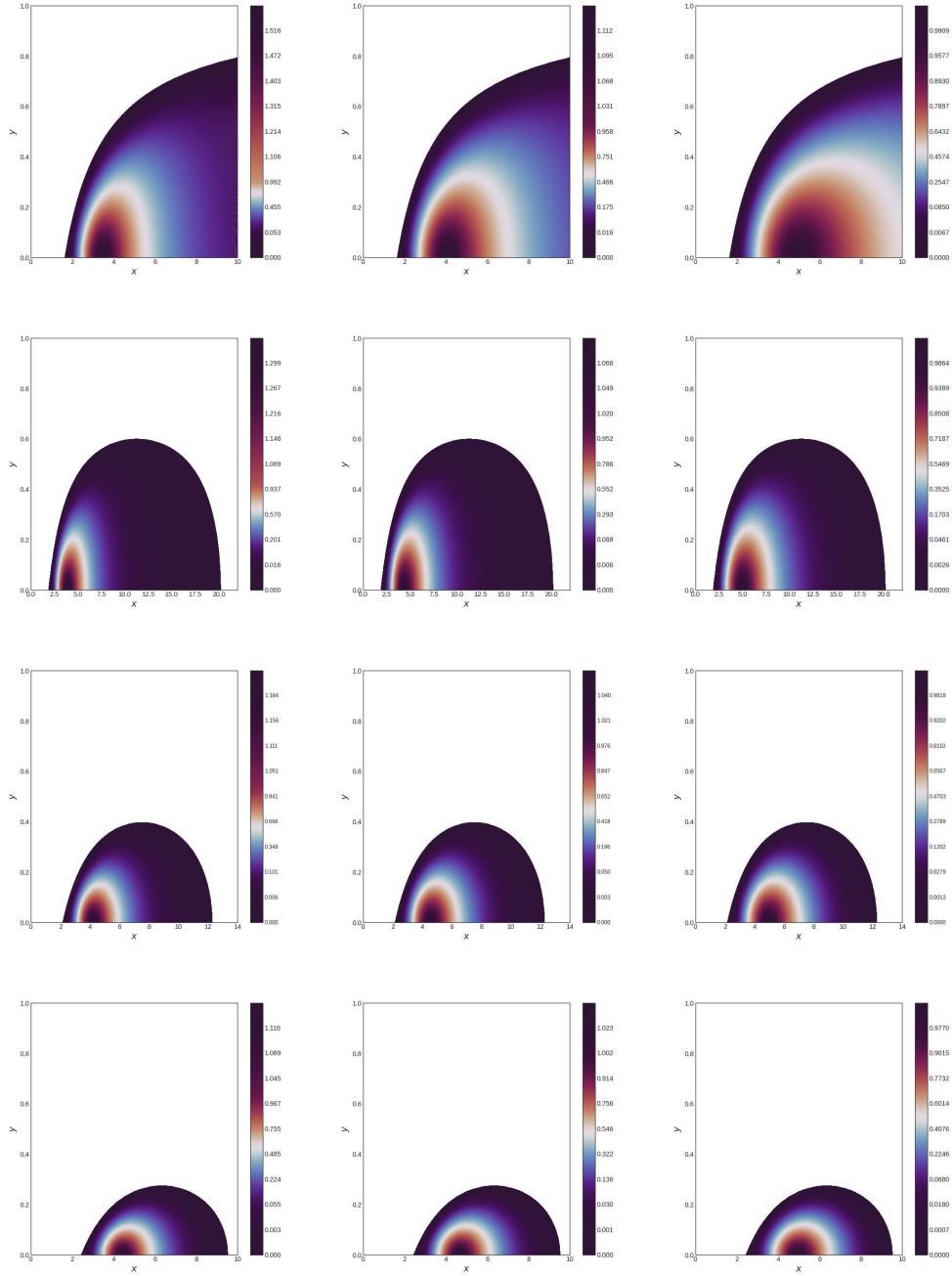


FIG. 5. Map of the rest-mass density distribution for $q = -0.4$. From the left to the right, the magnetisation parameter varies. The first column corresponds to $\beta_c = 10^{-3}$, second to $\beta_c = 1$ and third to $\beta_c = 10^3$. Also, the distribution of the specific angular momentum varies in rows. First row represents the constant specific angular momentum, the second row model 3, the third row model 2, and the last row shows model 1.

surfaces in general. However, the analysis on how δ affects the structure of the disc is in correlation with α that one can not study this contribution independently.

Finally, in Figure 11 we have explored the effect of the deformation parameter q on the structure of the disc with considering the variation of angular momentum distributions. In this case we have set magnetisation parameter to $\beta_c = 10^{-3}$. Each column corresponds to a chosen value of q . It starts with

a negative value $q = -0.4$ at the left, then $q = 0$, and a positive value $q = 1.5$ at the right. In the vertical direction, as in Figure 10, the distribution of the angular momentum is changing by making its parameters vary in the same way. In comparison to the Figure 10 it has seen that the deformed parameter q is more responsible for the radial extension of the disc.

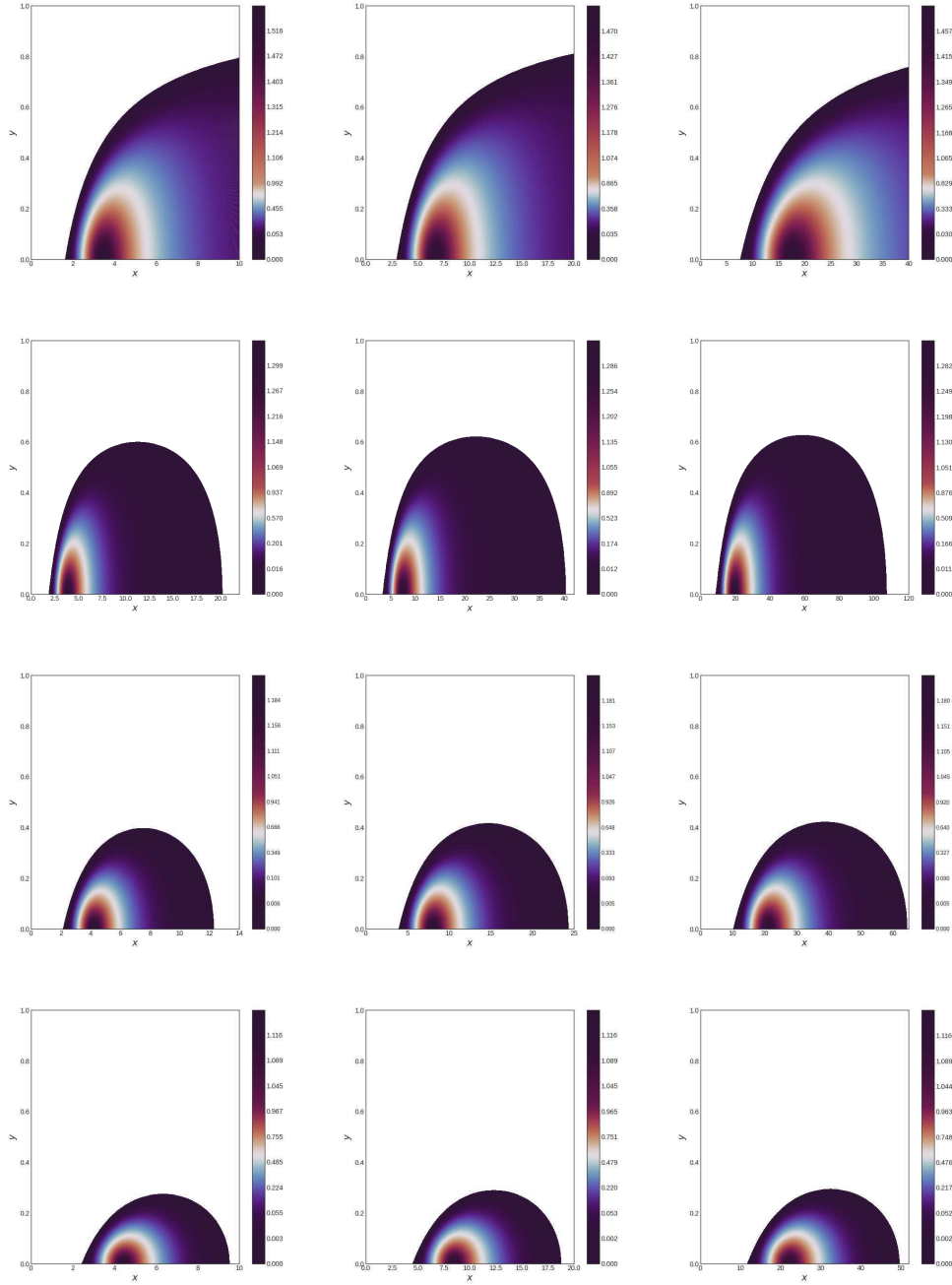


FIG. 6. Map of the rest-mass density distribution. From the left to the right the value of q varies. The column at the left shows $q = -0.4$, at the centre $q = 0$ and, at the right represents $q = 1.5$. Also, rows correspond to different distributions of the specific angular momentum. First row shows the constant specific angular momentum, the second row model 3, the third row model 2, and the last one shows model 1. The magnetisation parameter is set to be $\beta_c = 10^{-3}$ in all maps.

VII. SUMMARY AND CONCLUSION

In this paper, we analysed equilibrium sequences of magnetised, non-self-gravitating discs around a deformed compact object up to the quadrupole. This solution is described via the q -metric which is briefly explained in Section V.

In this procedure we combine the two existing approaches

of [10] combined with [11], also [10] combined with [13] to study the space-time generated by this deformed object via analysing the properties of the magnetic tori disc model around this object. Explicitly, on the one hand we followed the method in [10] to attach a dynamically toroidal magnetic field to the model. On the other hand, besides specific constant angular momentum distribution, we consider two models for

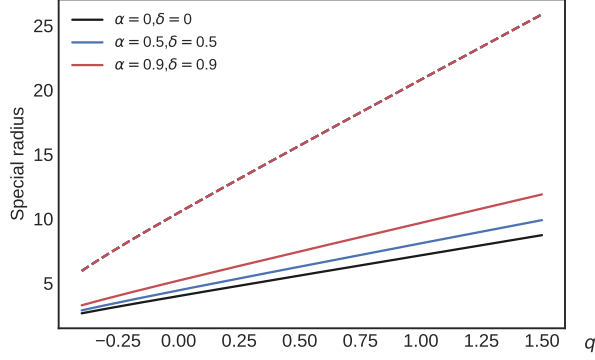


FIG. 7. Variation of the location of the cusp (solid lines) and the location of the centre (dashed line) as a function of q for the different distribution of specific angular momentum.

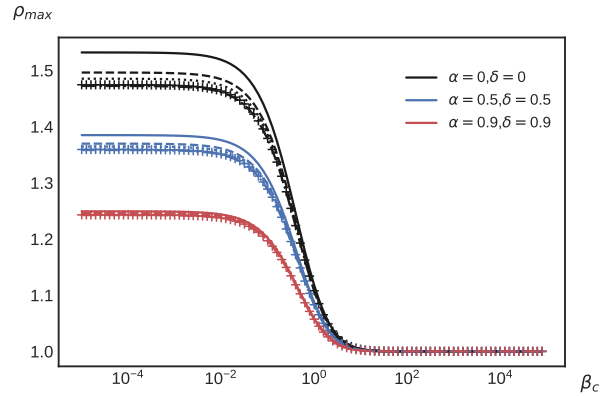
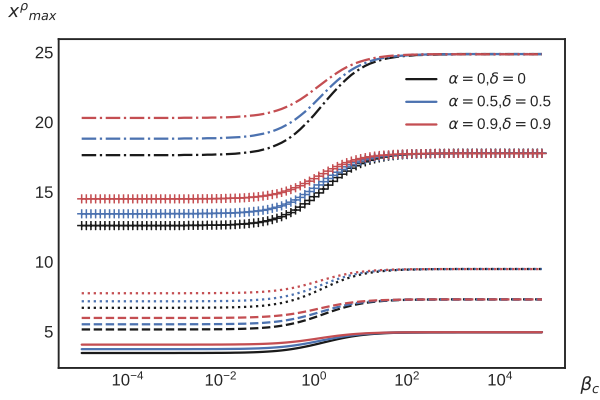


FIG. 8. Variation of the location and amplitude of the rest-mass density as a function of β_c , for three models of angular momentum profiles and five values of q . In this plot $q = -0.4$ and $q = -0.2$ are depicted in solid line and dashed line, $q = 0$ is shown in the dotted line, $q = 0.8$ and $q = 1.5$ are represented in crossed and dot-dashed lines respectively.

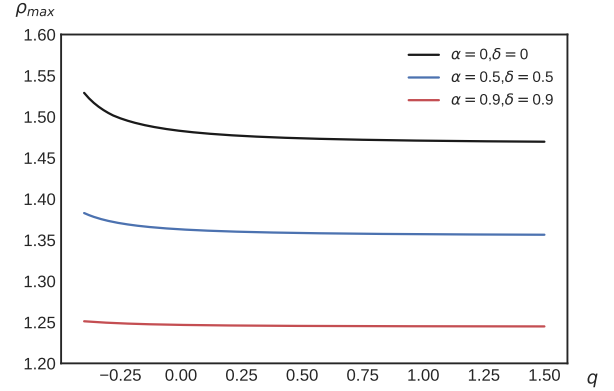
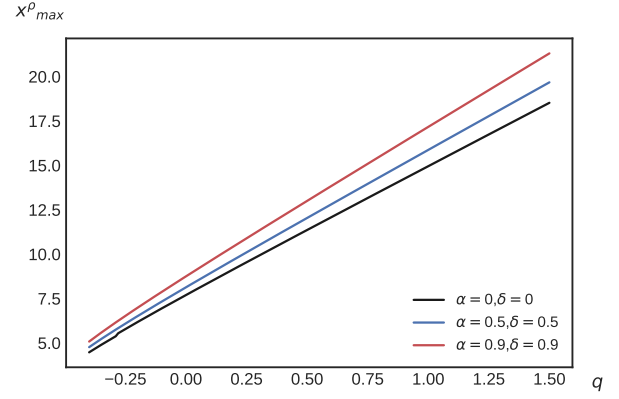


FIG. 9. Variation of the location and amplitude of the maximum of the rest-mass density in the equatorial plane as a function of q for three angular momentum profiles. The magnetisation parameter is set to be $\beta_c = 10^{-3}$

the non-constant distribution of angular momentum where the location and the morphology of the surfaces of equipotential can be computed, as introduced in [11] and [13], which have been briefly explained in Section IV. Also, the results are in good agreement with the result of the mentioned papers when we limited our attention to the vanishing quadrupole moment case.

We have analysed the influence of the magnetisation parameter β_c , the quadrupole parameter q and the angular momentum distributions on the structure of the magnetised thick disc model. We have shown that changing parameter β_c has a noticeable effect on the location and amplitude of the rest-mass density. In fact, a higher magnetic pressure, namely lower β_c , causes the matter to concentrate more in the inner part of the disc. Furthermore, in this case the range of isodensity contours is increasing which is compatible with the increase of rest-mass density in the inner part of the disc.

On the other hand, the deformed parameter q is responsible for the radial extension of the disc. namely, the greater we choose q , the more extended disc we have. Besides, the location of the rest-mass density is affected by quadrupole parameters, as it is an increasing function of q . On the contrary, its effect on the amplitude is reversed as it was expected. In

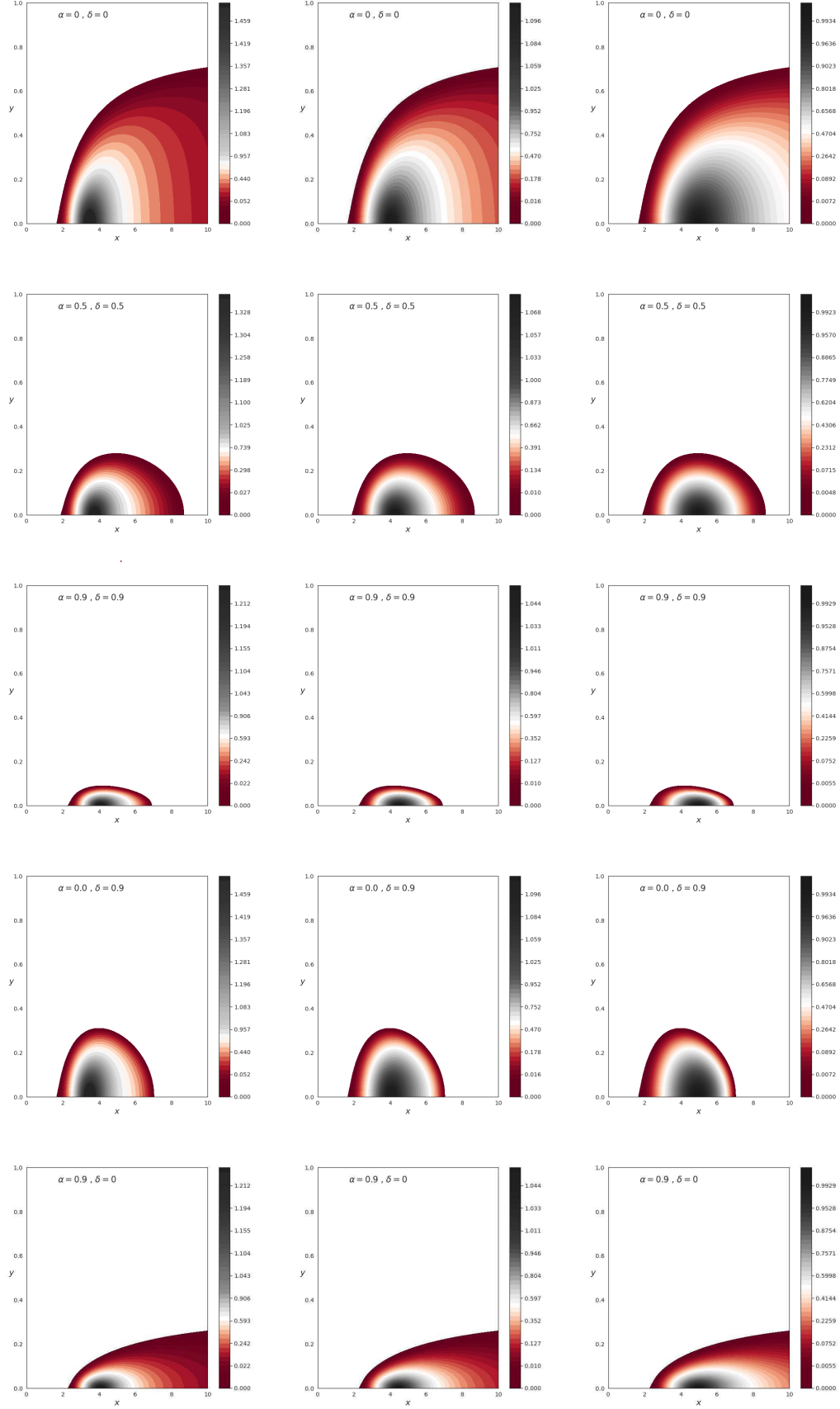


FIG. 10. Map of the rest-mass density distribution for $q = -0.4$. From the left to the right, the magnetisation parameter varies, namely 10^{-3} , 1 and 10^3 respectively. In rows the power index α and δ is changing. We have chosen these following pairs $(\alpha = \delta = 0)$, $(\alpha = \delta = 0.5)$, $(\alpha = \delta = 0.9)$, $(\alpha = 0, \delta = 0.9)$, $(\alpha = 0.9, \delta = 0)$ from the top to the bottom.

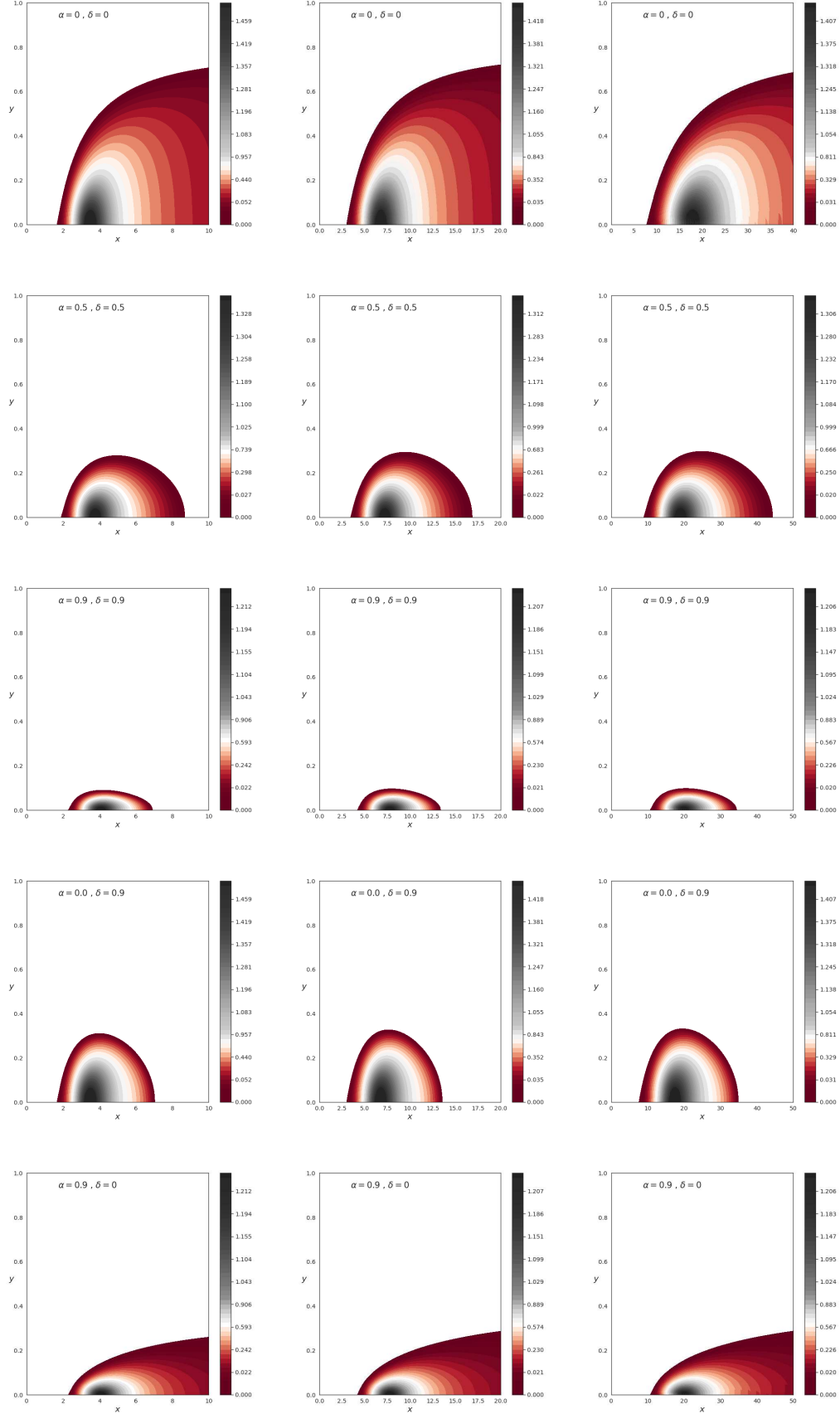


FIG. 11. Map of the rest-mass density distribution. From the left to the right, the parameter q varies. The column at the left shows $q = -0.4$, the middle $q = 0$ and the right represents $q = 1.5$. In rows the power index α and δ is changing. We have chosen these following pairs with the following pairs $(\alpha = \delta = 0)$, $(\alpha = \delta = 0.5)$, $(\alpha = \delta = 0.9)$, $(\alpha = 0, \delta = 0.9)$, $(\alpha = 0.9, \delta = 0)$ from the top to the bottom. Also, the magnetisation parameter is set to be $\beta_c = 10^{-3}$.

addition, we have chosen parameter $q = 0$ in models for comparison with the spherical case, which shows that the results are in good agreement with the mentioned literature.

Furthermore, we have explored the effects of different angular momentum distributions on the disc structure.

In the case of the power-law distribution of angular momentum, described in Subsection V A, we have shown that steeper angular momentum causes the disc to be more shrunk in the radial direction. Moreover, increasing in the steepness of the angular momentum profile, decreases the amplitude of the rest-mass density and pushes away the location of its maximum. In fact, it tends to spread the matter in the entire disc rather than to concentrate in the inner part as we have seen in Figure 6. Further in this case, the effect of having the steeper slope is similar to have a bigger positive quadrupole.

In addition, in the case of distribution of the angular momentum as a trigonometric function, explained in Subsection V B, we have shown that the pair (α, δ) affect strongly on the overall configuration of the disc. In fact, the α parameter is more responsible for the vertical direction of the disc, while parameter δ affects both the radial and the vertical extension.

However, in general the effects of δ on the structure of the disc is in correlation with the parameter α in a way that one can not study this contribution independently.

As a further step of this work, one can investigate the form of the barytropic equation of state. Also, one can consider the quadrupoles as the extra physical degree of freedom to the model that facilitate searching for the links to associate observational data to the astrophysical objects, like in the study of gravitational waves, or self-gravitating central objects. It is also of some interest to apply these models as the initial conditions in the numerical simulations and test their ability to account for observable constraints of astrophysical systems.

ACKNOWLEDGEMENTS

S.F. gratefully acknowledges Prof. Komissarov for his useful comment. The authors thank the research training group GRK 1620 "Models of Gravity", funded by the German Research Foundation (DFG).

-
- [1] M. A. Abramowicz, Theory of Level Surfaces Inside Relativistic: Rotating Stars. II., *Acta Astron* **24**, 45 (1974).
- [2] M. Kozłowski, M. Jaroszynski, and M. A. Abramowicz, The analytic theory of fluid disks orbiting the Kerr black hole., *Astron Astroph* **63**, 209 (1978).
- [3] M. Jaroszynski, M. A. Abramowicz, and B. Paczynski, Super-critical accretion disks around black holes, *Acta Astron* **30**, 1 (1980).
- [4] B. Paczyński and P. J. Wiita, Thick accretion disks and super-critical luminosities., *Astron Astroph* **500**, 203 (1980).
- [5] M. A. Abramowicz, M. Calvani, and L. Nobili, Thick accretion disks with super-Eddington luminosities, *Astrophys. J.* **242**, 772 (1980).
- [6] M. A. Abramowicz, Innermost parts of accretion disks are thermally and secularly stable, *Nature (London)* **294**, 235 (1981).
- [7] B. Paczynski, Thick Accretion Disks around Black Holes (Karl-Schwarzschild-Vorlesung 1981), *Mitteilungen der Astronomischen Gesellschaft Hamburg* **57**, 27 (1982).
- [8] B. Paczynski and M. A. Abramowicz, A model of a thick disk with equatorial accretion, *Astrophys. J.* **253**, 897 (1982).
- [9] S. A. Balbus and J. F. Hawley, A Powerful Local Shear Instability in Weakly Magnetized Disks. I. Linear Analysis, *Astrophys. J.* **376**, 214 (1991).
- [10] S. S. Komissarov, Magnetized tori around kerr black holes: analytic solutions with a toroidal magnetic field, *Monthly Notices of the Royal Astronomical Society* **368**, 993–1000 (2006).
- [11] L. Qian, M. A. Abramowicz, P. C. Fragile, J. Horák, M. Machida, and O. Straub, The Polish doughnuts revisited. I. The angular momentum distribution and equipressure surfaces, *Astron Astroph* **498**, 471 (2009), arXiv:0812.2467 [astro-ph].
- [12] S. Gimeno-Soler and J. A. Font, Magnetised Polish doughnuts revisited, *Astron Astroph* **607**, A68 (2017), arXiv:1707.03867 [gr-qc].
- [13] M. Wielgus, P. C. Fragile, Z. Wang, and J. Wilson, Local stability of strongly magnetized black hole tori, *MNRAS* **447**, 3593 (2015), arXiv:1412.4561 [astro-ph.HE].
- [14] P. C. Fragile and A. Sadowski, On the decay of strong magnetization in global disc simulations with toroidal fields, *MNRAS* **467**, 1838 (2017), arXiv:1701.01159 [astro-ph.HE].
- [15] Z. Kovács and T. Harko, Can accretion disk properties observationally distinguish black holes from naked singularities?, *Phys. Rev. D* **82**, 124047 (2010), arXiv:1011.4127 [gr-qc].
- [16] T. Harko, Z. Kovács, and F. S. N. Lobo, Thin accretion disks in stationary axisymmetric wormhole spacetimes, *Phys. Rev. D* **79**, 064001 (2009), arXiv:0901.3926 [gr-qc].
- [17] L. Rezzolla, O. Zanotti, and J. A. Font, Dynamics of thick discs around Schwarzschild-de Sitter black holes, *Astron Astroph* **412**, 603 (2003), arXiv:gr-qc/0310045 [gr-qc].
- [18] P. Slaný and Z. Stuchlík, Relativistic thick discs in the Kerr de Sitter backgrounds, *Classical and Quantum Gravity* **22**, 3623 (2005).
- [19] H. Kucáková, P. Slaný, and Z. Stuchlík, Toroidal configurations of perfect fluid in the Reissner-Nordström-(anti)-de Sitter spacetimes, *J. Cosmology Astropart. Phys.* **2011**, 033 (2011).
- [20] S. Faraji and A. Trova, Magnetized thick accretion disc around distorted static black hole, arXiv e-prints, arXiv:2011.00124 (2020), arXiv:2011.00124 [astro-ph.HE].
- [21] Z. Stuchlík and P. Slaný, Accretion disks in the Kerr-de Sitter spacetimes, in *RAGtime 4/5: Workshops on black holes and neutron stars*, edited by S. Hledík and Z. Stuchlík (2004) pp. 205–237.
- [22] H. Weyl, Zur gravitationstheorie, *Annalen der Physik* **359**, 117 (1917), <https://onlinelibrary.wiley.com/doi/pdf/10.1002/andp.19173591804>.
- [23] G. Erez and N. Rosen, The gravitational field of a particle possessing a multipole moment, *Bull. Research Council Israel* **Vol: Sect. F.8** (1959).
- [24] D. M. Zipoy, Topology of some spheroidal metrics, *Journal of Mathematical Physics* **7**, 1137 (1966).
- [25] B. H. Voorhees, Static axially symmetric gravitational fields, *Phys. Rev. D* **2**, 2119 (1970).
- [26] R. Geroch, Multipole Moments. II. Curved Space, *Journal of Mathematical Physics* **11**, 2580 (1970).

- [27] R. O. Hansen, Multipole moments of stationary space-times, *Journal of Mathematical Physics* **15**, 46 (1974).
- [28] H. Quevedo, General static axisymmetric solution of einstein's vacuum field equations in prolate spheroidal coordinates, *Phys. Rev. D* **39**, 2904 (1989).
- [29] V. S. Manko, On the description of the external field of a static deformed mass, *Classical and Quantum Gravity* **7**, L209 (1990).
- [30] N. Gürlebeck, Source integrals for multipole moments in static and axially symmetric spacetimes, *Phys. Rev. D* **90**, 024041 (2014).
- [31] B. Boisseau and P. S. Letelier, Relativistic multipoles and the advance of the perihelia, *General Relativity and Gravitation* **34**, 1077 (2002).
- [32] E. Guéron and P. S. Letelier, Geodesic chaos around quadrupolar deformed centers of attraction, *Phys. Rev. E* **66**, 046611 (2002).
- [33] F. López-Suspes and G. A. González, Equatorial circular orbits of neutral test particles in weyl spacetimes, *Brazilian Journal of Physics* **44**, 385 (2014).
- [34] S. Toktarbay and H. Quevedo, A stationary q-metric, *Gravitation and Cosmology* **20**, 252–254 (2014).
- [35] H. Quevedo, Multipole moments in general relativity —static and stationary vacuum solutions—, *Fortschritte der Physik/Progress of Physics* **38**, 733 (1990), <https://onlinelibrary.wiley.com/doi/pdf/10.1002/prop.2190381002>.
- [36] H. Quevedo and B. Mashhoon, Exterior gravitational field of a rotating deformed mass, *Physics Letters A* **109**, 13 (1985).
- [37] J. Castejon-Amenedo and V. S. Manko, On a stationary rotating mass with an arbitrary multipole structure, *Classical and Quantum Gravity* **7**, 779 (1990).
- [38] O. Semerák, Circular orbits in stationary axisymmetric spacetimes, *General Relativity and Gravitation* **30**, 1203 (1998).
- [39] H. Quevedo, Mass Quadrupole as a Source of Mass Naked Singularities, *International Journal of Modern Physics D* **20**, 1779 (2011), arXiv:1012.4030 [gr-qc].
- [40] H. Quevedo, Mass quadrupole as a source of naked singularities, *International Journal of Modern Physics D* **20**, 1779 (2011).
- [41] H. Quevedo, Exterior and interior metrics with quadrupole moment, *Gen. Rel. Grav.* **43**, 1141 (2011), arXiv:1003.4344 [gr-qc].
- [42] In fact, the Arnowitt-Deser-Misner mass which characterizes the physical properties of the exact solution also has the same expression and should be positive, also for stationary space-time it is equivalent to Komar mass.
- [43] A. M. Anile, *Relativistic fluids and magneto-fluids : with applications in astrophysics and plasma physics* (Oxford Univ. Press, 1989).
- [44] W. G. Dixon, *Special relativity: the foundation of macroscopic physics*. (Oxford Univ. Press, 1978).
- [45] M. Abramowicz, M. Jaroszynski, and M. Sikora, Relativistic, accreting disks., *Astron Astroph* **63**, 221 (1978).
- [46] The general relativistic version of the von Zeipel theorem states that for a toroidal magnetic field the surfaces of constant p coincide with the surfaces of constant w if and only if constant Ω and constant ℓ coincide [48, 49].
- [47] R. Okada, J. Fukue, and R. Matsumoto, A model of astrophysical tori with magnetic fields, *PASJ* **41**, 133 (1989).
- [48] H. von Zeipel, The radiative equilibrium of a rotating system of gaseous masses, *MNRAS* **84**, 665 (1924).
- [49] O. Zanotti and D. Pugliese, Von Zeipel's theorem for a magnetized circular flow around a compact object, *General Relativity and Gravitation* **47**, 44 (2015), arXiv:1412.6447 [gr-qc].